Journal Title: 2D Materials

Volume:
Issue:
Month/Year:
Pages:

Article Author: Hao et al

Article Title: Trion valley coherence in monolayer semiconductors

Notes:

Location:
Call No.:

Item #:

Requestor:

Susan Wright (swright)
Phone: x4635
325 Braodway
Applied Physics Div (x686)
Boulder, CO 80305

IOP Publishing 2D Mater. 4 (2017) 025105 https://doi.org/10.1088/2053-1583/aa70f9

2D Materials

PAPER

Trion valley coherence in monolayer semiconductors

RECEIVED
13 March 2017

REVISED
20 April 2017

ACCEPTED FOR PUBLICATION
4 May 2017

PUBLISHED
22 May 2017

Kai Hao[1], Lixiang Xu[1], Fengcheng Wu[1], Philipp Nagler[2], Kha Tran[1], Xin Ma[1], Christian Schüller[2], Tobias Korn[2], Allan H MacDonald[1], Galan Moody[3] and Xiaoqin Li[1]

[1] Department of Physics and Center for Complex Quantum Systems, University of Texas at Austin, Austin, TX 78712, United States of America
[2] Department of Physics, University of Regensburg, Regensburg 93040, Germany
[3] National Institute of Standards & Technology, Boulder, CO 80305, United States of America

E-mail: elaineli@physics.utexas.edu and galan.moody@nist.gov

Keywords: transition-metal dichalcogenides, valley coherence, trions, two-dimensional coherent spectroscopy

Supplementary material for this article is available online

Abstract

The emerging field of valleytronics aims to exploit the valley pseudospin of electrons residing near Bloch band extrema as an information carrier. Recent experiments demonstrating optical generation and manipulation of exciton valley coherence (the superposition of electron–hole pairs at opposite valleys) in monolayer transition metal dichalcogenides (TMDs) provide a critical step towards control of this quantum degree of freedom. The charged exciton (trion) in TMDs is an intriguing alternative to the neutral exciton for control of valley pseudospin because of its long spontaneous recombination lifetime, its robust valley polarization, and its coupling to residual electronic spin. Trion valley coherence has however been unexplored due to experimental challenges in accessing it spectroscopically. In this work, we employ ultrafast 2D coherent spectroscopy to resonantly generate and detect trion valley coherence in monolayer $MoSe_2$ demonstrating that it persists for a few-hundred femtoseconds. We conclude that the underlying mechanisms limiting trion valley coherence are fundamentally different from those applicable to exciton valley coherence.

Introduction

The energy extrema in the band structure of monolayer transition metal dichalcogenides (TMDs) occur at the K and K' points at the hexagonal Brillouin zone boundary. Broken spatial inversion symmetry and strong spin-orbit interactions introduce valley-contrasting physical properties that enable manipulation of the valley pseudospin degree of freedom (DoF) [1–7]. Most notably, electrons and holes residing at the K and K' valleys possess opposite spin, orbital magnetic moment, and Berry curvature [8]. This intrinsic link between the electronic properties and the valley index has led to novel concepts in the burgeoning field of valleytronics. A seminal example in monolayer and bilayer TMDs as well as bilayer graphene is the valley Hall effect, which provides an electrical probe of the valley index [9, 10].

Due to a sizable bandgap, the valley DoF in TMDs can be conveniently addressed and controlled optically. As with any binary quantum DoF, the valley pseudospin can be modeled as a two-level system and represented using the Bloch sphere shown in figure 1(a). Using right- and left-circularly polarized light, photo-excitation of electron–hole pairs (excitons) into the K and K' valleys is possible, generating valley polarization. Excitons can also be prepared into a quantum superposition between valleys using linearly polarized excitation, creating valley coherence. An upper limit on the exciton valley coherence time is imposed by its recombination lifetime, which is a few hundred femtoseconds in monolayer TMDs due to the large exciton oscillator strength [11, 12]. Furthermore, electron–hole exchange leads to faster exciton valley decoherence than that imposed by recombination [2, 13, 14]. A natural question arises: can one generate, detect, and manipulate the valley DoF via a different optical transition?

The charged exciton (trion) is a promising alternative to the exciton due to its longer lifetime, robust valley polarization, and coupling to the additional charge [15]. In molybdenum-based monolayers, the lowest-energy trion resonance is an inter-valley singlet state consisting of an electron–hole pair in one valley and an electron in the lowest conduction band in the other valley with opposite spin as shown in figure 1(b) [16–20]. Even after electron–hole recombination, the remaining electron may maintain definitive valley index and spin orientation, making the trion an attractive candidate to manipulate the valley DoF [21, 22]. Although

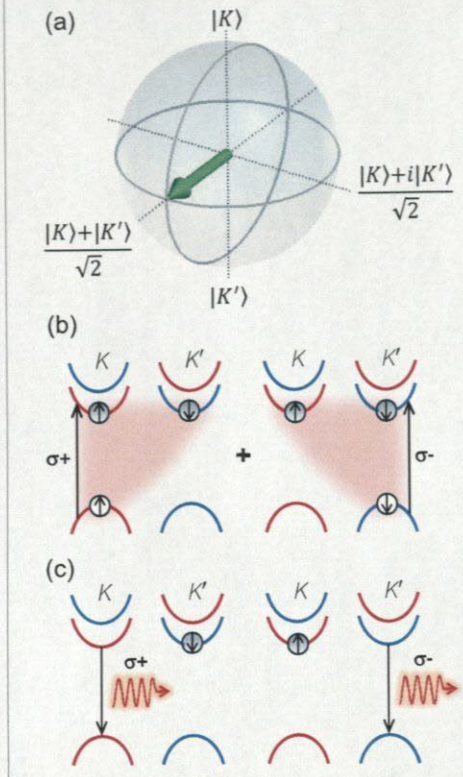

Figure 1. Trion valley coherence in monolayer $MoSe_2$. (a) Valley polarization and coherence are represented by a pseudospin vector on the Bloch sphere oriented along the north/south poles and in the equatorial plane, respectively. (b) Linearly polarized optical excitation can generate trion valley coherence between the lowest-energy negative trion states in $MoSe_2$. (c) Electron–hole recombination leads to a spin-photon entangled state due to the opposite residual electronic spins, preventing detection of the trion valley coherence in photoluminescence.

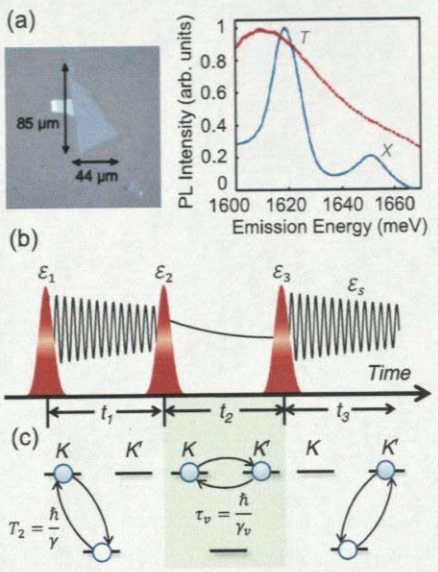

Figure 2. Resonant generation and detection of trion valley coherence. (a) Image of the $MoSe_2$ monolayer. The low temperature photoluminescence spectrum features trion and exciton emission at ~1620 meV and ~1650 meV, respectively. (b) Three pulses with variable delays and polarizations interact with the sample to generate a nonlinear four-wave mixing signal. (c) Cross-circularly polarized excitation and detection, in which the first and third (second and signal) pulses are left- (right-) circularly polarized. The quantum pathway corresponding to the generation, evolution, and detection of trion valley coherence is illustrated by the three-level energy diagram in the interaction picture.

linearly polarized optical emission has been used to conveniently monitor exciton valley coherence, the same technique is not applicable to trions. Following linearly polarized optical excitation, a coherent superposition of two trion valley configurations is created (figure 1(b)). Upon electron–hole recombination, one configuration becomes a σ^+ photon and spin-down electron while the other becomes a σ^- photon and spin-up electron (figure 1(c)). In contrast to the exciton, their linear superposition leads to a spin-photon entangled state $|\sigma^+\rangle|\downarrow\rangle+|\sigma^-\rangle|\uparrow\rangle$, which cannot be detected as linearly polarized emission due to the orthogonal spin states. For this reason, trion valley coherence has rarely been discussed in the existing literature, leaving a gap in our fundamental understanding of valley quantum dynamics in 2D materials.

Here, we provide a direct measurement of trion valley coherence in monolayer $MoSe_2$ using 2D coherent spectroscopy (2DCS), which is a three-pulse four-wave mixing technique [23]. A pair of optical pulses with opposite helicity resonantly creates a coherent superposition of two trions in opposite valleys. Trion valley coherence is read out by detecting the four-wave mixing signal generated by a time-delayed third optical pulse. We have obtained a complete set of measurements evaluating the trion and exciton valley coherence, interband optical coherence (coherent superposition between the ground and excited states), and recombination dynamics by choosing a variety of different polarization schemes and scanning pulse delays. This comprehensive picture of the coherent quantum dynamics associated with trions in monolayer $MoSe_2$ offers critical guidance for valley pseudospin manipulation.

Experiment methods and sample

Monolayer $MoSe_2$

A microscope image of our $MoSe_2$ sample is shown in figure 2(a). The sample is obtained by mechanical exfoliation onto an optically transparent sapphire substrate. A micro-photoluminescence intensity spectrum is presented in the right panel of figure 2(a), which is acquired using a linearly polarized pump at 1960 meV (633 nm) with the sample under vacuum at 20 K. Pronounced narrow-linewidth exciton and trion resonances are observed at ~1650 meV and ~1620 meV, respectively. For the trion we find similar photoluminescence intensity for orthogonal, linearly polarized detection angles (data not shown),

consistent with the expected negligible degree of linear polarization explained previously.

Optical 2D coherent spectroscopy

Optical 2DCS is a particularly powerful tool for probing the full coherent valley dynamics of excitons and trions in TMDs [11, 24, 25]. The technique employs a series of 30 fs pulses generated from a mode-locked Ti:sapphire oscillator at an 80 MHz repetition rate and with sufficient bandwidth to excite both the exciton and trion transitions. The laser output is split into four phase-locked pulses (figure 2(b)) using a platform of nested Michelson interferometers, enabling precision stepping of the pulse delays with ~1 fs resolution [26]. Three pulses are focused to a ~30 μm spot and interact with the monolayer to generate a four-wave mixing signal $\mathbf{E}_S(t_1, t_2, t_3)$. The signal field is spectrally resolved in transmission through heterodyne detection with a phase-locked local oscillator derived from the fourth pulse. The fluence of each pulse at the sample is kept below ~1 μJ cm^{-2} (~3 × 10^{11} excitons cm^{-2}) to remain in the $\chi^{(3)}$ regime and to minimize Auger-type recombination [27]. The valley coherence dynamics are obtained by recording the signal and scanning the delay t_2 between the second and third pulses while keeping the delay t_1 held fixed (figure 2(c)). The signal field is Fourier transformed with respect to t_2 to generate a 2D spectrum $\mathbf{E}_S(t_1, \hbar\omega_2, \hbar\omega_3)$, which correlates the zero-quantum frequencies of the system during the delay t_2 with the one-quantum (i.e. emission) frequencies of the system during the emission time t_3. A zero quantum spectrum provides access to the non-radiative valley coherence and lifetime dynamics of excitons and trions, which is unique but complementary in comparison to the more conventional one-quantum spectrum $[\mathbf{E}_S(\hbar\omega_1, t_2, \hbar\omega_3)]$ that probes interband optical coherence, coherent and incoherent couplings, and many-body states [11, 24, 25, 28].

Results and discussion

Isolating the individual quantum pathways associated with non-radiative valley coherence and population recombination is possible by selecting the helicity of the excitation pulses and detected signal. We first present valley coherence measurements in which the first and third pulses are left-circularly polarized (σ^+) and the second pulse and detected signal are right-circularly polarized (σ^-). The quantum pathways responsible for valley coherence can be understood within the framework of perturbation theory of the $\chi^{(3)}$ nonlinear response. As illustrated in figure 2(c), the first pulse creates a first-order coherent superposition between the crystal ground state and the trion in the K valley. After a delay t_1 (set to zero in the present experiments), the second pulse drives the system into a second-order non-radiative coherent superposition of the trion configurations in the K and K' valleys. The trion valley coherence evolves during the delay t_2, after which the third pulse converts the valley coherence to a third-order optical coherence in the K' valley, which then radiates as the signal. We note that this particular polarization scheme of the interacting fields is inaccessible in the commonly used pump-probe technique. Using this sequence, we are able to isolate valley coherence among all possible third-order quantum mechanical pathways.

The resulting zero-quantum spectrum for cross-circular polarization is shown in figure 3(a). The spectrum features two resonances at emission energies of ~1619 meV and ~1649 meV corresponding to the trion valley coherence (T) and exciton valley coherence (X), respectively. Because the transitions in the K and K' valleys are degenerate [5, 6], the valley pseudospin vector does not precess about the Bloch sphere during t_2 and instead its magnitude decays exponentially with a valley decoherence rate γ_v (valley coherence time $\tau_v = \hbar/\gamma_v$). As a result, the resonances in figure 3(a) are at the origin of the zero-quantum axis ($\hbar\omega_2$) with a half-width at half-maximum (HWHM) equal to γ_v. Lorentzian fits to the lineshapes (figures 3(b) and (c)) reveal a valley coherence time for the trion and exciton of $\tau_v^T = 230$ fs ($\gamma_v^T = 2.9$ meV) and $\tau_v^X = 140$ fs ($\gamma_v^X = 4.8$ meV), respectively.

The similar order-of-magnitude for the exciton and trion valley coherence times is a surprising result because they have different recombination and valley properties. The large exciton oscillator strength and non-radiative decay processes result in ultrafast recombination with a lifetime $T_1^X = 210$ fs, placing an upper limit on the exciton valley coherence time. Furthermore, electron–hole exchange accelerates exciton valley decoherence by breaking the two-fold valley degeneracy through the Maialle–Silva–Sham mechanism [13, 14]. Likewise, both ultrafast population relaxation and electron–hole exchange lead to rapid exciton valley depolarization from an initial exciton valley polarization of 50% within ~350 fs under resonant excitation conditions (see figures 3(d)–(f) and the supplemental information (stacks.iop.org/TDM/4/025105/mmedia)). For trions, recombination and valley depolarization are expected to be slower compared to excitons. In the sample studied in this work with a low doping density, our measurements indeed yielded a trion recombination time $T_1^T = 4.7$ ps, a higher degree of initial valley polarization (~75%), and a subsequent valley depolarization time of ~3 ps (see figures 3(d)–(f) and the supplemental information). Slower trion valley depolarization is expected, as we now explain. First, unlike excitons with zero center-of-mass momentum, the inter-valley trions at the K and K' valleys carry opposite center-of-mass momentum. Second, electron–hole exchange causes valley depolarization via annihilation of an electron–hole pair in one valley and creation of another pair in the other valley. This process would correspond to the formation of an intra-valley trion in $MoSe_2$, which has a higher energy. The momentum conservation and energy up-conversion requirements reduce the trion inter-valley scattering rate.

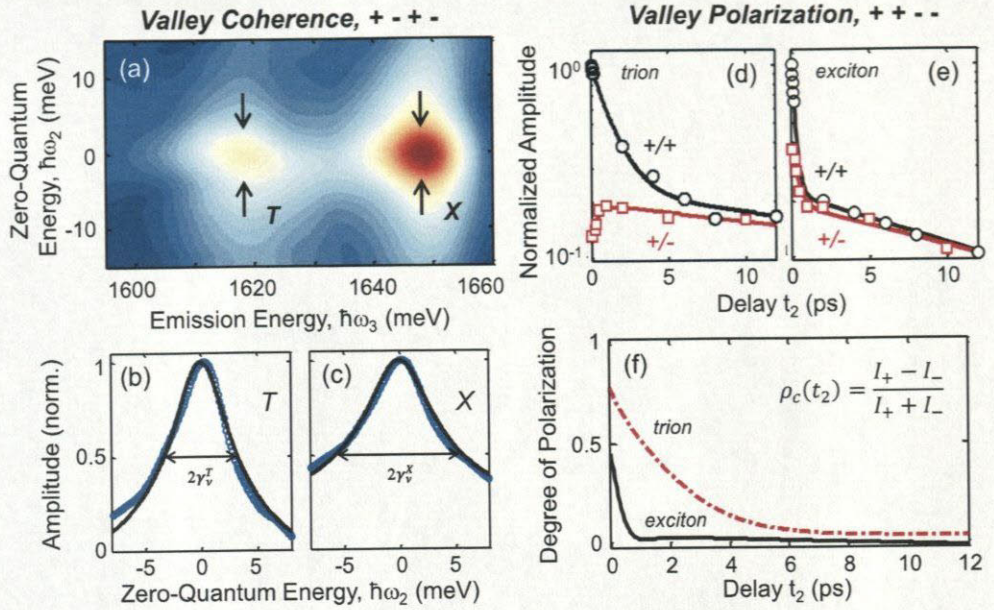

Figure 3. Inter-valley coherence and valley polarization dynamics. (a) Optical 2DCS zero-quantum spectrum acquired using the cross-circular polarization scheme. Two peaks are present at the emission energies of the exciton (X) and trion (T), respectively. (b) and (c) The half-width at half-maximum of Lorentzian fit functions (solid lines) to the lineshapes along the zero-quantum axis $\hbar\omega_2$ yields the valley decoherence rate γ_v (valley coherence time $\tau_v = \hbar/\gamma_v$), equal to $\gamma_v^T = 2.9$ meV ($\tau_v^T = 230$ fs) and $\gamma_v^X = 4.8$ meV ($\tau_v^X = 140$ fs) for the trion and exciton, respectively. Valley polarization dynamics for the (d) trion and (e) exciton obtained from one-quantum spectra acquired for co- and cross-circular polarization. (f) Bi-exponential fits to the amplitudes in (d) and (e) are used to determine the degree of circular polarization versus t_2.

The fact that the trion valley coherence time is nearly an order-of-magnitude shorter than its recombination lifetime and valley depolarization dynamics suggests that trions are more susceptible to pure dephasing from interactions with their local fluctuating environment. We verify this point with additional experiments in which the first delay t_1 is scanned while the second delay t_2 is held fixed. The nonlinear signal is Fourier transformed with respect to t_1, which produces a one-quantum spectrum $\mathbf{E}_S(\hbar\omega_1, t_2, \hbar\omega_3)$ that correlates the excitation and emission energies of the system during the delays t_1 and t_3. The excitation pulses and signal are co-circularly polarized so that we are evaluating inter-band optical coherence of excitons and trions in one valley. The resulting one-quantum spectrum is shown in figure 4(a). The diagonal line indicates excitation and emission at the same energy; the two diagonal peaks at ~1619 meV and ~1649 meV correspond to the non-linear response associated with the trion and exciton transitions, respectively. The peaks are elongated along the diagonal, which indicates moderate inhomogeneous broadening. The HWHM of the lineshapes along the cross-diagonal direction [29], shown in figure 4(b), is approximately equal to the homogeneous linewidth γ, which is inversely proportional to the interband optical coherence time T_2. We measure for the trion and exciton $T_2^T = 510$ fs ($\gamma^T = 1.3$ meV) and $T_2^X = 470$ fs ($\gamma^X = 1.4$ meV), respectively [11]. In general, the optical coherence times are related to the recombination lifetime through $(T_2)^{-1} = (2T_1)^{-1} + (T_2^*)^{-1}$, where T_2^* is the pure dephasing time that describes optical decoherence from elastic scattering processes that do not affect the population.

These results confirm our expectations: exciton optical decoherence is lifetime limited ($T_2^X \approx 2T_1^X$), whereas trion optical decoherence is dominated by pure dephasing from its environment ($T_2^T \ll T_1^T$). This observation supports the view that trion features in the optical properties of doped TMDs may be viewed as coming from exciton dressing by a Fermi sea, with internal quantum fluctuations, rather than a single electron [30, 31]. Alternatively, pure dephasing might also arise from scattering of trions from charged surface adsorbates, defects, or impurities in the monolayer TMD and the substrate through the long-range screened Coulomb interaction. In a quasi-2D GaAs quantum well, the screened Coulomb interaction is stronger for the trion compared to the exciton [32], which is consistent with the presence (absence) of pure dephasing for the trion (exciton) observed here.

A summary of the quantum dynamics of excitons, trions, and their associated valley index is provided in table S1, which highlights the key differences between the exciton and trion. From density matrix calculations of the valley dynamics for a simple three-level V-system (see figure 2(c)), one can write a general expression for the valley coherence time as $(\tau_v)^{-1} = (T_1)^{-1} + (\tau_v^*)^{-1}$, where τ_v^* represents scattering events that lead to pure valley decoherence without affecting the valley polarization. We note that the factor of one-half in front of

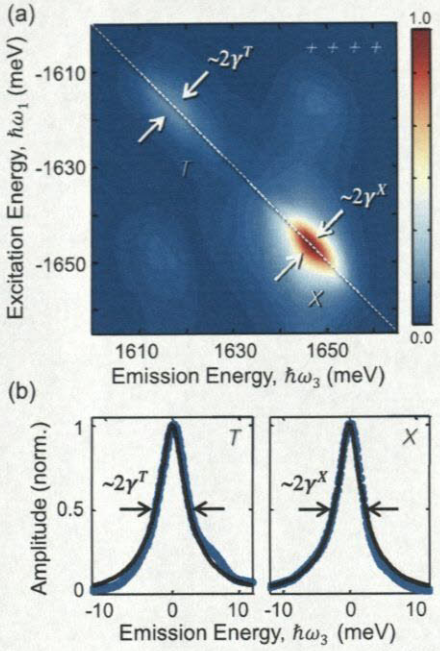

Figure 4. Interband optical coherence dynamics. (a) Optical 2DCS one-quantum spectrum acquired using co-circular polarization. The peaks on the diagonal line correspond to excitation and emission at the exciton and trion resonances. (b) The resonance lineshapes along the cross-diagonal direction are fit with Lorentzian functions to obtain the homogeneous linewidth (coherence time) $\gamma^T = 1.3$ meV ($T_2^T = 510$ fs) and $\gamma^X = 1.4$ meV ($T_2^X = 470$ fs) for the trion and exciton, respectively.

T_1 for the expression for interband optical decoherence is absent in the expression above for valley coherence, since recombination from either valley contributes to valley decoherence. With the assumption that scattering events in the K and K' valleys are uncorrelated, we can express the valley coherence time as $(\tau_v)^{-1} = (T_1)^{-1} + 2(T_2^*)^{-1}$ [33,34], i.e. trion valley coherence is governed by recombination and pure optical dephasing processes. While this simple model doesn't fully capture the exciton valley coherence dynamics due to additional dephasing from the electron–hole exchange interaction, it is entirely compatible with the singlet trion for which inter-valley exchange is suppressed. We find that $\tau_v^T \approx T_2^{*,T}/2$, which supports our assertion that pure optical dephasing is the dominant valley decoherence mechanism for the trion.

Conclusions

Based on the new knowledge of the mechanisms governing trion valley decoherence, we suggest several ways to extend the valley coherence time. Our key observation that trion valley decoherence is primarily from pure dephasing arising from interactions with the surrounding environment suggests that the valley coherence time can be enhanced, possibly by lowering the density of carriers. Furthermore, intra-valley trions in monolayer WSe_2 have been recently demonstrated to exhibit exceptionally robust valley polarization under resonant excitation [35]. This particular trion resonance may also exhibit extended valley coherence time. More importantly, the excitation of valley-selective trions serves to optically initialize the spin/valley index of free electrons in monolayer TMDs. A tantalizing hypothesis is that after electron–hole recombination, the residual electron bound to the trion composite quasiparticle could maintain its valley polarization and coherence. This is consistent with the nanosecond long spin coherence time [21,22] observed in monolayer TMDs and should be tested in future experiments. Finally, adiabatic excitation schemes may be applied to realize valley qubit rotations similar to coherent control experiments performed on electron spins in quantum dots [36,37].

Acknowledgments

The theoretical and experimental collaboration is made possible via SHINES, an Energy Frontier Research Center funded by the U.S. Department of Energy (DoE), Office of Science, Basic Energy Science (BES) under award # DE-SC0012670. KH, FW, LX, XL, and AHM have all received support from SHINES. AHM also acknowledges support from Welch Foundation F-1473. XL also acknowledges the support from NSF EFMA-1542747, a Humboldt fellowship, and Welch Foundation F-1662. PN, CS and TK gratefully acknowledge technical assistance by S Bange and financial support by the German Research foundation (DFG) via GRK 1570 and KO3612/1-1.

References

[1] Jones A M *et al* 2013 *Nat. Nanotechnol.* **8** 634
[2] Hao K *et al* 2016 *Nat. Phys.* **12** 677
[3] Wang G, Glazov M M, Robert C, Amand T, Marie X and Urbaszek B 2015 *Phys. Rev. Lett.* **115** 117401
[4] Wang G, Marie X, Gerber I, Amand T, Lagarde D, Bouet L, Vidal M, Balocchi A and Urbaszek B 2015 *Phys. Rev. Lett.* **114** 097403
[5] Wang G, Marie X, Liu B L, Amand T, Robert C, Cadiz F, Renucci P and Urbaszek B 2016 *Phys. Rev. Lett.* **117** 187401
[6] Ye Z, Sun D and Heinz T 2017 *Nat. Phys.* **13** 26–9
[7] Schmidt R *et al* 2016 *Phys. Rev. Lett.* **117** 077402
[8] Xu X, Yao W, Xiao D and Heinz T F 2014 *Nat. Phys.* **10** 343
[9] Lee J, Mak K F and Shan J 2016 *Nat. Nanotechnol.* **11** 421
[10] Mak K F, McGill K L, Park J and McEuen P L 2014 *Science* **344** 1489
[11] Hao K, Xu L, Nagler P, Singh A, Tran K, Dass C K, Schüller C, Korn T, Li X and Moody G 2016 *Nano Lett.* **16** 5109
[12] Poellmann C, Steinleitner P, Leierseder U, Nagler P, Plechinger G, Porer M, Bratschitsch R, Schüller C, Korn T and Huber R 2015 *Nat. Mater.* **14** 889
[13] Wu F, Qu F and MacDonald A H 2015 *Phys. Rev.* B **91** 075310
[14] Yu T and Wu M W 2014 *Phys. Rev.* B **89** 205303
[15] Wang G, Bouet L, Lagarde D, Vidal M, Balocchi A, Amand T, Marie X and Urbaszek B 2014 *Phys. Rev.* B **90** 075413
[16] Mak K F, He K, Lee C, Lee G H, Hone J, Heinz T F and Shan J 2013 *Nat. Mater.* **12** 207
[17] Ross J S *et al* 2013 *Nat. Commun.* **4** 1474

[18] Liu C H, Frenzel A J, Pilon D V, Lee Y-H, Ling X, Akselrod G M, Kong J and Gedik N 2014 *Phys. Rev. Lett.* **113** 166801
[19] Singh A, Moody G, Wu S, Wu Y, Ghimire N J, Yan J, Mandrus D G, Xu X and Li X 2014 *Phys. Rev. Lett.* **112** 216804
[20] Singh A *et al* 2016 *Phys. Rev.* B **93** 041401
[21] Yang L, Sinitsyn N A, Chen W, Yuan J, Zhang J, Lou J and Crooker S A 2015 *Nat. Phys.* **11** 830
[22] Song X, Xie S, Kang K, Park J and Sih V 2016 *Nano Lett.* **16** 5010
[23] Cundiff S T, Bristow A D, Siemens M, Li H, Moody G, Karaiskaj D, Dai X and Zhang T 2012 *IEEE J. Sel. Top. Quantum Electron.* **18** 318
[24] Dey P, Paul J, Wang Z, Stevens C E, Liu C, Romero A H, Shan J, Hilton D J and Karaiskaj D 2016 *Phys. Rev. Lett.* **116** 127402
[25] Moody G *et al* 2015 *Nat. Commun.* **6** 8315
[26] Bristow A D, Karaiskaj D, Dai X, Zhang T, Carlsson C, Hagen K R, Jimenez R and Cundiff S T 2009 *Rev. Sci. Instrum.* **80** 073108
[27] Moody G, Schaibley J and Xu X 2016 *J. Opt. Soc. Am.* B **33** C39
[28] Hao K *et al* 2017 *Nat. Commun.* **8** 15552
[29] Siemens M E, Moody G, Li H, Bristow A D and Cundiff S T 2010 *Opt. Express* **18** 17699
[30] Efimkin D K and MacDonald A H 2017 *Phys. Rev.* B **95** 035417
[31] Sidler M, Back P, Cotlet O, Srivastava A, Fink T, Kroner M, Demler E and Imamoglu A 2017 *Nat. Phys.* **13** 255–61
[32] Manassen A, Cohen E, Ron A, Linder E and Pfeiffer L N 1996 *Phys. Rev.* B **54** 10609
[33] Moody G, Singh R, Li H, Akimov I A, Bayer M, Reuter D, Wieck A D and Cundiff S T 2013 *Solid State Commun.* **163** 65
[34] Yajima T and Taira Y 1979 *J. Phys. Soc. Japan* **47** 1620
[35] Singh A *et al* 2016 *Phys. Rev. Lett.* **117** 257402
[36] Calarco T, Datta A, Fedichev P, Pazy E and Zoller P 2003 *Phys. Rev.* A **68** 012310
[37] Simon C-M *et al* 2011 *Phys. Rev. Lett.* **106** 166801